Optical Spectroscopy Using Gas-Phase Femtosecond Laser Filamentation

Johanan Odhner and Robert Levis

Department of Chemistry and Center for Advanced Photonics Research, Temple University, Philadelphia, Pennsylvania 19122; email: rjlevis@temple.edu

Annu. Rev. Phys. Chem. 2014. 65:605–28

First published online as a Review in Advance on January 9, 2014

The *Annual Review of Physical Chemistry* is online at physchem.annualreviews.org

This article's doi: 10.1146/annurev-physchem-040513-103708

Keywords

nonlinear spectroscopy, standoff Raman, backward lasing, white light, quantum wake

Abstract

Femtosecond laser filamentation occurs as a dynamic balance between the self-focusing and plasma defocusing of a laser pulse to produce ultrashort radiation as brief as a few optical cycles. This unique source has many properties that make it attractive as a nonlinear optical tool for spectroscopy, such as propagation at high intensities over extended distances, self-shortening, white-light generation, and the formation of an underdense plasma. The plasma channel that constitutes a single filament and whose position in space can be controlled by its input parameters can span meters-long distances, whereas multifilamentation of a laser beam can be sustained up to hundreds of meters in the atmosphere. In this review, we briefly summarize the current understanding and use of laser filaments for spectroscopic investigations of molecules. A theoretical framework of filamentation is presented, along with recent experimental evidence supporting the established understanding of filamentation. Investigations carried out on vibrational and rotational spectroscopy, filament-induced breakdown, fluorescence spectroscopy, and backward lasing are discussed.

1. INTRODUCTION

The phenomenon of femtosecond laser pulse filamentation in atomic and molecular gases leads to spectacular reshaping of the pulse in the temporal, spectral, and spatial domains, providing new capabilities for performing molecular spectroscopy. The physics of laser filamentation has been reviewed previously (1–3); here we focus on the aspects of filamentation that lend themselves to spectroscopic investigations as a result of laser pulse reshaping. Temporal reshaping of the pulse envelope due to the interplay between nonlinear propagation effects leads to self-shortening of the pulse to durations as short as a few femtoseconds, or just several oscillations of the electromagnetic field at a carrier frequency of 375 THz (800 nm). Self-shortening is accompanied by the generation of coherent spectral bandwidth spanning the visible and infrared (IR) regions of the spectrum. These few-cycle laser pulses can impulsively excite rotational and vibrational motion in molecules, generating a coherent wave packet comprising a superposition of internal molecular states, which is described by

$$\Psi(t) = \Sigma_i \psi_i(t, \theta_i), \tag{1}$$

where $\Psi(t)$ is the time-dependent wave packet, which is described by a set of eigenstates, ψ_i, of the molecule having a definite phase relationship between them, θ_i. In the case of propagation in air, the filament forms rotational and vibrational quantum wakes (4, 5) that propagate forward at the group velocity of the exciting pulse and continue to recur at a particular point in space until dephasing eliminates the coherence. The rotational and vibrational coherences excited in a filament can be imprinted on a second laser beam propagating through the wake of the filament to provide spectroscopic information about the medium. Rotational revivals in air form the dominant contribution to the index of refraction (6–8) and can either focus or defocus light propagating through the medium. The high intensity in the filament will also ionize the medium, resulting in a weak, underdense plasma string that can be used, for instance, to trigger and guide a high-voltage discharge (9). Finally, the high intensity of the pulse can be used to ablate and vaporize solid materials, serving as a source of atomic emission for filament-induced breakdown spectroscopy (10), and in fact, this led directly to the intact vaporization of molecules for atmospheric pressure mass spectrometry and the laser electrospray mass spectrometry technique (11–13).

A femtosecond laser pulse propagating in a gaseous medium at a sufficiently high peak power undergoes self-focusing (14), also known as Kerr lensing. Self-focusing occurs when the power contained in the laser pulse exceeds the critical power for self-focusing in the medium, given by $P_{\text{crit}} = 3.77\lambda_0^2/8\pi n_0 n_2$ for a Gaussian beam, where λ_0 is the laser wavelength, n_0 is the linear refractive index at the laser wavelength, and n_2 is the coefficient of the nonlinear refractive index (15). Above the critical power, the refractive index gradient caused by the optical Kerr effect exceeds the effect of diffraction on the laser beam, causing the beam to contract. Under these conditions, the beam rapidly focuses, leading to the generation of ever-higher intensities. Catastrophic beam collapse is avoided when the intensity of the laser pulse becomes high enough to ionize the medium, generating free electrons that provide a negative contribution to the index of refraction gradient across the beam profile. The index of refraction contribution of the free electron distribution is given by $-\omega_p^2/2\omega^2$, where $\omega_p = [4\pi e^2 n_e(I)/m_e]^{1/2}$ is the plasma frequency, ω is the optical frequency, $n_e(I)$ is the intensity-dependent electron density, and m_e is the mass of an electron. The radially dependent electron density distribution produced by the intensity distribution of the laser thus provides a defocusing mechanism. A dynamic equilibrium between the Kerr focusing and plasma defocusing effects leads to extended propagation of the beam at high intensities ($\sim 10^{13}$ W cm^{-2} in air), typically over a distance of the order of meters in length, which results in a visible propagation channel originating from bremsstrahlung and fluorescence emission. The so-called white-light plasma string formally constitutes the region of the femtosecond laser filament. The interplay of

the optical field with the instantaneous electronic, delayed nuclear (for molecular species), and ionization responses of a medium provides a simple and robust means to produce few-cycle laser pulses (16, 17). In turn, one can use the few-cycle laser pulse thus generated to interact with all modes of nuclear motion known, ranging from very slow rotational modes to the highest-frequency ground electronic state vibrational mode possible (in H_2). Such pulses can be used as ultrafast probes of chemical processes and also allow standoff detection in experiments ranging from the detection of Raman-active modes to laser-induced breakdown spectroscopy. With respect to performing spectroscopy, white-light filamentation also has the benefit of decreased noise in comparison with the driving pulse due to the phenomenon of intensity clamping in the filament (10, 14, 18).

Gas-phase filaments have been formed using driving lasers with wavelengths ranging from the ultraviolet (UV) (19, 20), to the near-IR (14), to the mid-IR (21–23). The power threshold for filamentation in the UV is lower than in the near-IR range because the index of refraction for air increases with laser frequency, and there is an inverse relationship between n_0 and P_{crit}, as described above. In the mid-IR range, one has access to the anomalous dispersion regime, and the threshold for filamentation may again decrease. Experiments are currently underway to explore this regime using ytterbium laser systems delivering multimillijoule energies in the mid-IR (23, 24).

2. HISTORY OF FILAMENTATION

In 1962, Askaryan (25) predicted laser filamentation in the condensed phase shortly after the invention of the laser, and it was first observed using a ruby laser by Hercher (26) in 1964. The visible damage tracks seen upon propagation of the laser through optical glass were interpreted as self-trapping of the beam, initiated by the optical Kerr effect, with subsequent propagation in a self-induced dielectric waveguide (27). An alternate model was later proposed that considered the sequential focusing of different intensity slices of a laser pulse onto the propagation axis, giving the appearance of one continuous filament (28). This model was later verified for the case of nanosecond pulses (see 29). Subsequent work showed that filamentation is a complex, dynamic phenomenon, and researchers made growing experimental and theoretical progress toward understanding nanosecond and picosecond pulse self-focusing in the following years (15, 29). One important aspect of filamentation, noted early on, is the remarkable frequency broadening that occurs. In 1970, Alfano & Shapiro (30–32) first reported the formation of a continuous spectrum spanning thousands of wave numbers (continuum generation) during filamentation by using picosecond pulses in glasses, crystals, and atomic liquids. This observation was markedly different than self-phase modulation induced by nanosecond pulses, with characteristic spectral modulations that suggested the formation of very short optical transients (10^{-13}–10^{-15} s) caused by shocks formed through self-steepening (33) or optical breakdown (34). Such experiments served as a means to conveniently generate bright, coherent, spectrally broad radiation that could be used directly for optical spectroscopy with picosecond (35) and femtosecond (36) time resolution.

Filamentation in atmospheric gases was initiated by nanosecond experiments in the late 1980s that considered long-range self-focusing (e.g., 37). In 1987, Kühlke et al. (38) reported the spectral broadening of focused femtosecond laser pulses in air with evidence of self-focusing. Following the innovation of chirped-pulse amplification by Strickland & Mourou (39) and the development of titanium-sapphire-based femtosecond chirped-pulse amplifiers in the early 1990s (40–42), Braun et al. (14) observed self-channeling of 200-fs laser pulses at peak powers slightly higher than 10 GW in air. In this seminal paper, the authors reported whole-beam self-focusing that generated 80-μm-diameter filaments, with approximately 750 μJ of energy in each filament, which propagated over several tens of meters. They also reported white-light generation, conical off-axis emission, and clamping of the laser intensity at approximately 7×10^{13} W cm^{-2}, as calculated

from the measured beam parameters assuming a constant pulse duration. The origin of femtosecond laser filamentation over long distances (~20 m) was identified as a balance between self-focusing induced by the optical Kerr effect and ionization induced by defocusing, similar to the observations of Umstader & Liu (43) several years earlier for focused-beam geometries. Braun et al.'s report ignited the intensive investigation of laser filamentation, with applications ranging from the control of high-voltage discharges to remote sensing (44–47).

Early theoretical work predicted that laser filamentation would produce sharp temporal features that could result in pulses shorter than the original driving pulse. In fact, some simulations suggested that self-shortening from ~25 fs to a single optical cycle could be possible using an 800-nm laser pulse (48). As detailed below, this self-shortening occurs automatically with an extraordinary degree of robustness in the laser filamentation process. In addition, the mode profile of the filament is normally a nearly perfect Gaussian radial intensity distribution, even with poor incident pulse characteristics (49). The inherent self-shortening and mode cleaning serve as motivation for much of the spectroscopic work reviewed here.

3. GENERAL MECHANISM OF FEMTOSECOND FILAMENTATION

The moving-focus model of filamentation (15, 28, 29) was shown to be accurate for long (nanosecond and subnanosecond) pulses 20 years prior to the observation of femtosecond laser filaments. The observations of Braun et al. (14) and subsequent investigations (45–47, 50) raised new questions about the mechanism of filamentation by femtosecond-duration pulses. In particular, the moving-focus model was found to be unable to accurately predict the extension of filaments beyond the linear focus when formed in focusing geometries (50). The self-channeling, or self-waveguiding, model also failed over long distances, owing, in first approximation, to the absorption of the laser field during plasma formation, thus disrupting the static balance of the Kerr focusing and plasma defocusing nonlinearities (51). These inconsistencies led to Mlejnek et al.'s (52) proposal of a new propagation paradigm termed "dynamic spatial replenishment." The dynamic spatial replenishment model recognizes the spatial and temporal effects of self-focusing and plasma defocusing on the pulse envelope during propagation. These combined effects initially cause the trailing portion of the pulse to be spatially defocused, at which point plasma generation is curtailed and self-focusing again becomes dominant, a process that can occur multiple times until the peak power drops below that needed for refocusing. Thus, filamentation is sustained by a succession of focusing and defocusing events that depend on the pulse characteristics and medium parameters. The focusing and defocusing events are not static in the sense that focusing does not balance defocusing, as occurs in a soliton-like solution (51–54). Although these results show that filamentation (in the gas phase) is largely dominated by the processes of self-focusing and plasma defocusing, they also show that even small changes in either the propagation medium or the driving laser pulse significantly affect the pulse propagation. Furthermore, a host of linear and nonlinear effects contributes to the complex propagation dynamics, including dispersion, diffraction, instantaneous and delayed (rotational/vibrational) Kerr-like nonlinearities, self-steepening, space-time focusing, plasma generation, and multiphoton absorption. This fact is born out by the incredible diversity of measurements made in the nearly two decades since the study of high-power femtosecond laser filamentation was initiated by Braun et al. (14).

4. THEORETICAL DESCRIPTION OF FILAMENTATION

A brief discussion of the theoretical description of pulse propagation is constructive in understanding the relevant participating linear and nonlinear processes that govern the filamentation dynamics. The nonlinear envelope equation (55), a generalized form of the so-called nonlinear

Schrödinger equation, has been widely used to describe the propagation of ultrashort pulses in various media (see 56, 57, and references therein). Here we follow the recent derivation (56) and discuss the implications of the various nonlinear effects that are important for spectroscopic applications of femtosecond laser filamentation. The nonlinear envelope equation for the forward component of the field, E, with a central frequency ω_0 in the retarded time frame ($t = t - z/v_g$) can be written

$$\frac{\partial}{\partial z}E = \frac{i}{2k_0}T^{-1}\nabla_{\perp}^2 E + iDE + i\frac{\omega_0}{c}n_2 T\left[(1-x_K)|E|^2 + x_K\int_{-\infty}^{t} R(t-t')\left|E(t')\right|^2 dt'\right]E$$
$$-i\frac{k_0}{2n_0^2\rho_c}T^{-1}\rho E - \frac{\sigma}{2}\rho E - \frac{U_i W(I)(\rho_{nt}-\rho)}{2|E|^2}E, \tag{2}$$

$$T = \left(1 + \frac{i}{\omega_0}\frac{\partial}{\partial t}\right), \tag{3a}$$

$$\frac{\partial}{\partial t}\rho = W(I)(\rho_{\mathrm{nt}} - \rho) + \frac{\sigma(\omega_0)}{U_i}\rho|E|^2 - f(\rho), \tag{3b}$$

where the first term on the right-hand side of Equation 2 accounts for diffraction, the second term for dispersion, the third term for instantaneous and delayed Kerr effects, the fourth for photoionization, the fifth for collisional ionization, and the last for absorption losses due to photoionization. Space-time focusing and self-steepening are taken into account through the operator T (Equation 3a) in front of the diffraction and Kerr terms, respectively. The Raman response function $R(t-t')$ accounts for the rotational response in molecular gases such as nitrogen and oxygen and can be described using models that are relatively simple (58) or more sophisticated (6, 59–61), depending on the desired accuracy and the timescale of interest. Equation 3b defines the evolution of the plasma density, ρ, on the right-hand side in terms of the intensity-dependent photoionization rate, $W(I)$, collisional ionization, and electron recombination/attachment to adjacent ions. Additional parameterization to include quintic and higher-order Kerr effects has been extensively considered (see 62–68).

Generalized nonlinear Schrödinger equation simulations have been used to garner significant insight into the mechanism of femtosecond laser filamentation (1, 56), particularly in the area of pulse self-shortening. Brée et al. (69, 70) recently showed that the essential dynamics of filamentation can be understood using a reduced model considering only the instantaneous Kerr effect and plasma generation:

$$\frac{\partial}{\partial z}E = \frac{i}{2k_0 r}\frac{\partial}{\partial r}r\frac{\partial}{\partial r}E + i\frac{\omega_0}{c}n_2|E|^2 E - i\frac{1}{2\rho_c}\frac{\omega_0}{c}\rho(I)E, \tag{4}$$

$$\rho(I) = \rho_{\mathrm{nt}}\left(1 - \exp\left[-\int_{-\infty}^{t} dt' W(I(t'))\right]\right), \tag{5}$$

where radial coordinates have been used. With these approximations, the mechanisms of pulse reshaping during filamentation have been restricted to include only spatial effects. Brée et al.'s results demonstrated that the evolution of a femtosecond pulse in a single filament occurs in three steps: plasma-induced pulse breaking, isolation of one of the on-axis temporal peaks, and subsequent temporal compression. Self-focusing causes a rapid increase in the on-axis intensity and ionization of the medium at the leading edge of the pulse. The radially dependent degree of ionization leads in turn to spatial defocusing of the trailing edge. These effects produce an asymmetric pulse profile on the optical propagation axis and a temporally shortened pulse on the

optical axis due to the generation of blue frequencies from the rapidly changing electromagnetic field as a function of time, dE/dt. Subsequently, if the defocused trailing edge of the pulse has sufficient power for self-focusing, refocusing will occur, generating a characteristic multipeak temporal profile in the center of the pulse. Even as the trailing edge is refocusing, the leading edge is attenuated on the optical propagation axis by diffraction, dispersion, and absorption. Ultimately, only the trailing portion of the pulse survives and is temporally shortened by the preservation of the high-intensity on-axis component, which resists diffraction by the optical Kerr effect. This interpretation of the dynamic spatial replenishment model is confirmed by simulations performed using Equation 2, which show that a similar dynamic reshaping of the pulse occurs, as predicted by the reduced model (69).

5. HIGHER-ORDER KERR HYPOTHESIS

In 2009, a report challenged the standard model of filamentation as a dynamic balance between Kerr focusing and plasma defocusing, by claiming the measurement of higher-order terms in the nonlinear polarizability using time-resolved pump-probe polarization spectroscopy. Loriot et al. (71) measured the transient birefringence imposed by a strong pump pulse on a weak probe pulse with a relative polarization of 45° in a heterodyne-detected configuration and observed that the overall phase accumulation (or index of refraction) of the electronic contribution to the signal became negative for high pump intensities. The subsequent field-free rotational wave-packet revivals observed in molecular gases allowed the decoupling of the rotational contribution to the instantaneous polarization. The authors attributed the negative phase contribution to the saturation and inversion of the nonlinear refractive index through the optical Kerr effect and modeled it using a Taylor expansion of the Kerr terms up to eighth (n_8) order for nitrogen, oxygen, and air and tenth (n_{10}) order in argon. Loriot et al.'s results suggested that saturating higher-order Kerr terms could compete with or even replace plasma as the primary defocusing mechanism that balances self-focusing in a filament.

This report sparked a heated debate over both the measurement itself and the fundamental quantum mechanical behavior of an electron in a strong laser field. Shortly after the so-called higher-order Kerr effect (HOKE) was proposed (71), Wahlstrand et al. (72) provided an alternate interpretation of Loriot et al.'s transient birefringence data, attributing the observed sign inversion to plasma-induced birefringence that occurred through two-beam coupling. Further measurements of the nonlinear optical responses of N_2 and the noble gases using spectral interferometry showed that the electronic response remains positive well beyond the threshold for ionization (8, 20, 72). The resolution of the discrepancy between the transient birefringence measurement and these results was the finding that the authors of Reference 71 neglected the cross-phase modulation term originating from a spatial ionization grating that couples pump photons into the probe field direction, giving rise to a net polarization rotation. Spectrally resolved transient birefringence measurements made in the same configuration as the original measurement (71) showed that the ionization grating model reproduced the sign inversion of the birefringence for degenerate pump and probe frequencies, but not for nondegenerate pump and probe frequencies, and that the inversion scaled with the expected rate for multiphoton ionization at the frequency used in the measurement (73). A subsequent investigation at 800 nm using degenerate spectral interferometry and spectrally resolved transient birefringence confirmed these findings and provided a rigorous treatment of the effects governing pump-probe experiments in the strong-field regime (74). These experiments demonstrated that the original transient birefringence measurements (71) were misinterpreted. Time-dependent Schrödinger equation (TDSE) calculations on atomic hydrogen revealed that the standard models of femtosecond filamentation (i.e., models incorporating either multiphoton

ionization or tunnel ionization without higher-order Kerr contributions) fit the TDSE calculations reasonably well, whereas the HOKE model and an additional parameterization of the HOKE model fail to adequately reproduce the TDSE results (75). Further investigations are underway.

6. EXPERIMENTAL MEASUREMENT OF PROPAGATION DYNAMICS AND FILAMENT PROPERTIES

6.1. Impulsive Vibrational Excitation Measurements

In situ measurements testing theoretical predictions of femtosecond pulse propagation dynamics in a gas-phase filament were first accomplished using a spectroscopic method (76) in which the longitudinal dynamics of laser filamentation was measured using impulsive stimulated Raman scattering (ISRS) (77) from molecular vibrations. The filament wake was probed using a picosecond laser pulse along the propagation axis, z, to determine the extent of self-shortening as a function of the longitudinal propagation of the beam. Pulse self-shortening in the filament leads to impulsive excitation of each Raman-active vibrational mode present in the medium (77), in this case air, when the vibrational period is comparable to or longer than the self-shortened pulse. The detected impulsively excited Raman scattering signal along the probe beam path is given by the following expression:

$$S_{\mathrm{ISRS}}(\tau) = \int_{-\infty}^{\infty} dt \left|E_{\mathrm{pr}}(t)\right|^2 \left| \int_{-\infty}^{\infty} dt' \left|E_{\mathrm{pu}}(t+\tau-t')\right|^2 \chi_{\mathrm{vib}}(t) \right|^2, \qquad (6)$$

where $E_{\mathrm{pu}}(t)$ and $E_{\mathrm{pr}}(t)$ are the pump (filament) and probe electric fields, and $\chi_{\mathrm{vib}}(t)$ is the linear response function associated with the polarizability of individual vibrational modes. For air, the major constituent molecular species present are nitrogen, oxygen, and water vapor. In the case of O_2, the vibrational Raman shift of 1,554 cm^{-1} corresponds to a vibrational period of 21.5 fs; similarly, N_2 ($\omega_{\mathrm{vib}}/2\pi c = 2{,}330\ \mathrm{cm}^{-1}$) and H_2O ($\omega_{\mathrm{vib}}/2\pi c = 3{,}650\ \mathrm{cm}^{-1}$) have vibrational periods of 14.3 fs and 9.1 fs, respectively.

To meet the requirements for ISRS, the exciting laser pulse must exhibit a sufficiently high spectral power density to excite the Raman transition of the molecule. In addition, the pulse must contain an overall temporal structure that (*a*) is shorter than the period of the Raman mode to be excited and (*b*) does not have a multipeak profile that would result in destructive interference of the Raman wave packet. For an ultrashort (>50 fs) pulse producing a single filament under forced focusing conditions, numerical simulations predict that pulse breakup will not lead to the formation of more than two or three subpulses (70) and that isolation of a single subpulse is not an unusual outcome, suggesting that pulse shortening can be effectively monitored by measuring the amplitudes of the different Raman modes excited in the filament as a function of longitudinal position.

Employing a 1.9-mJ, sub-50-fs laser pulse focused by an $f = 2.27$-m lens in air to generate a white-light filament, investigators measured the Raman response of N_2, O_2, and H_2O. The appearance of the Raman signal before the geometric focus in **Figure 1*b*** reveals the influence of space-time focusing and self-steepening, which initially shortens the pulse so as to be able to excite both O_2 and N_2. The pulse then undergoes dynamic changes in structure after the nonlinear focus, which leads to oscillations in the Raman signal, before refocusing efficiently compresses the laser pulse, resulting in an increase of two to three orders of magnitude in the Raman signal strength from O_2 and N_2 and the appearance of the H_2O Raman peak.

Measurement of the combined electronic and atomic emissions and molecular fluorescence from the filament (termed plasma emission below) as a function of propagation distance provides

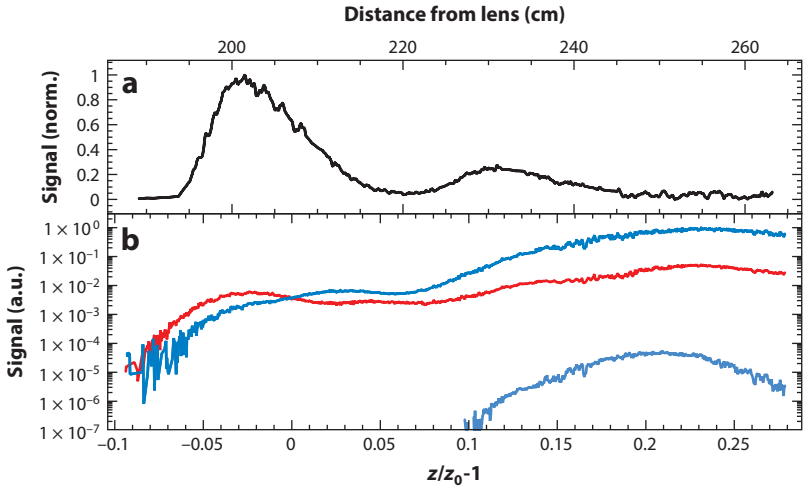

Figure 1

(*a*) Integrated fluorescence profile of a filament generated by a 1.9-mJ, sub-50-fs laser pulse in air focused by an $f = 2.27$-m lens. (*b*) Longitudinally resolved Raman signal from air. The intensities of the vibrational features for oxygen, nitrogen, and water are shown in red, dark blue, and light blue, respectively. Figure adapted with permission from Reference 76, copyright 2010 by the American Physical Society.

additional information regarding the position and intensity of the laser radiation in the filament. Such measurements made under the same filamentation conditions as the Raman measurements described above reveal two distinct focusing events during filamentation. The intensity of the plasma emission shown in **Figure 1*a*** is primarily a function of the radial fluence profile and the local pulse duration, and as a result, only general dynamics can be inferred from the data.

The spectral measurements provide evidence for pulse shortening but do not uniquely determine the temporal pulse shape with respect to the envelope and phase. Measuring the impulsive excitation of a particular vibrational mode with a given period is not sufficient to determine the duration or temporal structure of the filamenting laser pulse. Many more vibrational frequencies would be required to uniquely determine the phase and amplitude dynamics as a function of propagation distance.

6.2. Transient-Grating Cross-Correlation FROG Measurement of Propagation Dynamics

Direct measurement of the spectral amplitude and phase of a pulse undergoing filamentation using conventional pulse characterization methods is challenging because the intensity in the filament channel is sufficiently high so as to destroy optical components inserted in the beam path. Extraction of a small portion of the filament using an optic at grazing incidence is possible (78, 79), but the filament then passes through a solid material, altering its phase characteristics. The phase and amplitude information is crucial for validating simulations and for developing new spectroscopic probes based on filamentation.

To determine the temporal amplitude and phase of a pulse undergoing filamentation, researchers have performed transient-grating cross-correlation frequency-resolved optical gating (TG-XFROG) measurements. In this method, a transient grating is created in an inert gas (argon) by crossing two weak pulses, forming an optical interference pattern (**Figure 2**). An instantaneous

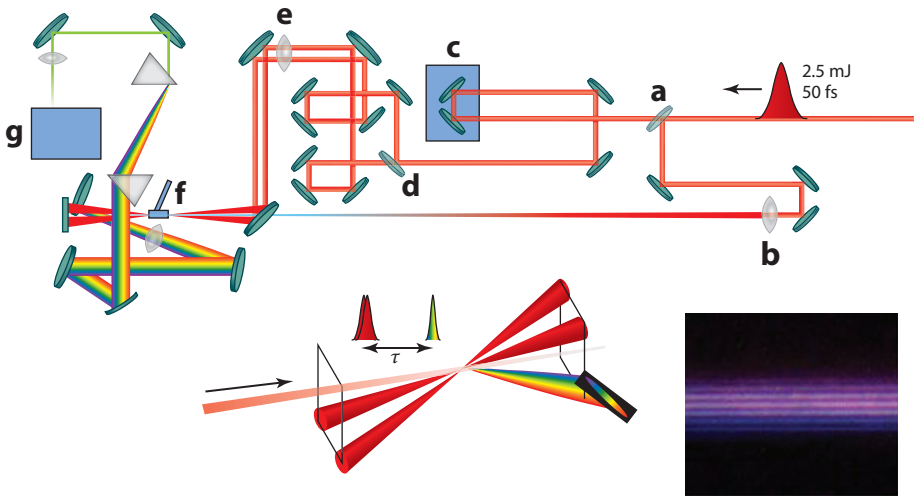

Figure 2

Experimental arrangement for transient-grating cross-correlation frequency-resolved optical gating (TG-XFROG) measurements of a filament: (*a*) 80/20 beam splitter, (*b*) $f = 2.27$-m lens, (*c*) delay stage, (*d*) 50/50 beam splitter, (*e*) $f = 0.5$-m lens, (*f*) argon jet, and (*g*) USB spectrometer. The interference pattern generated by overlapping two intense pulses in air is shown in the lower right. Figure taken from Reference 138.

polarization is then induced in the inert gas to create a real grating at a specific point in space and time. The filament then diffracts off the grating, and the diffracted light is measured using a spectrometer. The intensity of the probe beams is kept below the ionization threshold, thus avoiding the creation of a persistent plasma grating that would compromise the measurement. The spectrogram generated by measuring the diffracted filament light as a function of time delay between the filament and the probe pair provides the input to the FROG inversion algorithm used to extract the spectral (temporal) phase and amplitude at that particular position along the propagation axis of the filament. These measurements, repeated at different locations along the filament propagation path by translating the filament-generating lens, provide the temporal phase and amplitude dynamics of the pulse undergoing filamentation. In the preliminary measurements shown here, the distance from the focusing lens is fixed and the power of the incident beam is varied to understand its role in pulse compression.

Figure 3 shows the TG-XFROG retrievals made at a distance of $z = 255$ cm from the $f = 2.27$-m lens as a function of laser power, for which the maximum self-shortening is observed for a pulse energy of ~2 mJ. The relative time axes of the retrieved pulses are referenced on the position of a weak subpulse several hundreds of femtoseconds away from the main pulse, which is unaffected by the filamentation process. The intensity is provided in units of P_{crit}, which is taken to be 10 GW in air (80). As the power of the laser is increased, the pulse shifts forward in time as a result of plasma-induced defocusing at the back of the pulse. The double-peaked pulse profile observed at powers above P_{crit} is attributed to refocusing of the trailing edge of the pulse. At $3P_{crit}$, the refocusing tail dominates the temporal profile and significant blue-side broadening has occurred, extending the spectral edge to approximately 600 nm. The temporal amplitude of the pulse measured using the maximum power available here ($3P_{crit}$) reveals that the pulse self-shortens from 50 fs to 17 fs full width at half maximum with a 5-fs edge. These results are in qualitative agreement with the simulations of Brée et al. (69, 70, 81).

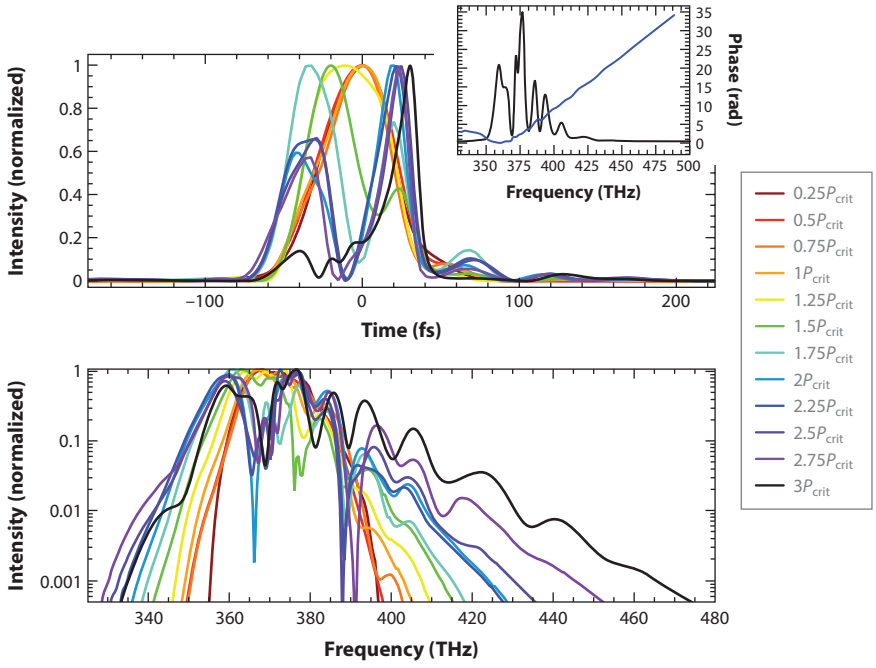

Figure 3

Filament (*a*) temporal and (*b*) spectral profiles (normalized intensities) versus input power measured 255 cm from the 2-m lens. (*Inset*) The linear spectrum and phase of the filament pulse at $3P_{crit}$. Figure taken from Reference 138.

6.3. Intensity Clamping and Mode Cleaning

As noted in Section 3, a laser undergoing self-focusing will eventually create a plasma that balances the Kerr lens to form an extended filament in which the intensity is limited to a value related to the ionization rate of the medium. To first approximation, this occurs when $n_2 I \approx n_e(I)/2n_{crit}$, where n_{crit} is the critical plasma density (14, 82). Estimates of the clamping intensity have been consistently placed at around several tens of terawatts for femtosecond laser filamentation since the earliest experiments. Because the Kerr effect and the ionization rate in turn depend on the atomic or molecular composition of the gas and the wavelength of the laser pulse, the dynamic balance in the filament will vary accordingly. Fluorescence emission has been used extensively to characterize filament propagation and intensity clamping (18, 83) because of the straightforward relationship with the intensity of the exciting laser pulse, although it does not have the spatial resolution to disentangle the radial pulse characteristics.

Studies have shown that intensity clamping leads to comparable or better pointing stability (84) and energy stability (85–87), even for higher-order processes such as four-wave mixing and third-harmonic generation. Filaments produce highly stable fluorescence emission (88). As intensity clamping can mediate the intensity and energy fluctuations inherent in the laser source, this immediately leads to better signal-to-noise characteristics in the beam as the shot-to-shot fluctuations in intensity are reduced in comparison with measurements made using the initial laser beam out of the cavity. Intensity clamping has been shown to be pressure independent (89), and this observation remains valid even at very high pulse energies (90, 91), although multiple filamentation plays a dominant role in this case. In addition to intensity clamping, the filament

beam automatically generates a nearly perfect spatial mode (49, 92). Again, this serves to improve the source as a means for probing chemical signatures.

7. SPECTROSCOPIC INVESTIGATIONS WITH FILAMENT SOURCES

The unique self-shortening and intensity clamping properties of laser filamentation in air have enabled several interesting new measurements on molecules, including rotational, vibrational, fluorescence, optical breakdown, terahertz sensing, and single-shot rotational measurements. Pulse self-shortening combined with four-wave mixing in a variety of gaseous media provides ultrashort laser pulses with bandwidths spanning 150 nm to 14 μm (85, 93–102). This allows temporal and spectral measurements that exceed the characteristics possible with conventional amplified laser pulses. In addition, the intensity clamping allows measurements with higher signal to noise in a given number of laser shots in comparison with conventional laser sources.

7.1. Rotational Spectroscopy

Excitation of rotational wave packets in molecular gases can strongly influence the propagation of a time-delayed probe pulse in the wake of a filament. A linearly polarized pulse will exert a torque on an isotropic distribution of linear molecules that have differing polarizability between the principal axes, leading to an induced interaction Hamiltonian, given by

$$H_{\text{ind}} = -\frac{1}{4}E^2\left(\alpha_{\|} - \alpha_{\perp}\right)\cos^2\theta, \tag{7}$$

where E is the electric field; $\alpha_{\|}$ and $\alpha_{\perp}$ are the components of the polarizability parallel and perpendicular to the principal axis, respectively; and θ is the angle between the principal axis and the polarization of the laser field (103). This torque causes the molecules to align while the laser is on and then produces periodic field-free molecular alignments in the medium after the laser pulse passes. The rotational wave packet thus created has a phase velocity equal to that of the pulse, propagating through the medium close to the speed of light. This propagating alignment, and its accompanying transient change in the index of refraction, has been termed a quantum wake (4).

Calegari et al. (104) first observed the effect of filament-induced impulsive rotational excitation on a weak, copropagating probe laser pulse. Strong spatial confinement and simultaneous spectral broadening and shifting were observed at delays corresponding to rotational revivals. The authors then further investigated the spectral and spatial reshaping of a probe pulse and compared it with numerical simulations (105). The alignment maxima and minima were correlated with parallel and perpendicularly oriented probe pulse data by comparing the spectrally integrated signal to the induced alignment $\langle\cos^2\theta\rangle$ calculated for nitrogen. They also observed the expected revival-induced birefringence imprinted on the probe pulse. In that experiment, crossed polarizers were used to determine the amount of polarization rotation in the probe beam due to the anisotropic polarizability introduced by the rotational alignment.

The effect of a preformed rotational quantum wake on the filamentation of a laser pulse has also been investigated. Varma et al. (4) showed that the filamentation of a pulse can be controlled by the timing delay between a rotational quantum wake excited by a moderately intense pump pulse and a probe pulse having sufficient power to produce a filament. At the well-defined revival times at which the molecules undergo alignment and antialignment, radially symmetric indices of refraction are created that can serve to focus or defocus the high-energy probe beam. Varma et al. (4, 106) reported that a filament can be trapped or destroyed by a molecular quantum wake, providing a possible enhancement to filament properties such as length and plasma density.

The propagation of intense filament pulses also leads to a nonlinear polarization anisotropy through the instantaneous (electronic) response as well as the delayed (rotational, vibrational, and ionization) responses of the medium. Experimental measurements of filament-induced birefringence were first reported for the case of pump-probe overlap in argon (107) and air (108) and subsequently in air resulting from rotational revivals by Marceau et al. (109). Using the filament-induced birefringence as a probe, Marceau et al. were able to track the revivals of oxygen and nitrogen in air and extract the rotational revival times, in agreement with previous measurements. In these experiments, the linearly polarized pump and probe beams were prepared with 45° rotation in their respective polarization directions. Whenever rotational alignment occurred, the polarizability of the medium became anisotropic, causing a slight rotation of the plane of polarization of the probe laser radiation. Such polarization rotation is typically detected using a pair of crossed polarizers, in which the geometry of the first polarizer defines the plane of polarization of the incident probe radiation and the second, placed at 90°, measures any polarization rotation. The measurements can be acquired either in a homodyne configuration in which the intensity ($|E|^2$) is measured or in a heterodyne configuration in which the electric field (E) is measured. For these cases, the signal is respectively proportional to

$$I_{\mathrm{sig}}^{\mathrm{hom}}(\tau) \propto \left[\langle \cos^2\theta \rangle_{\varphi(\tau)} - \frac{1}{3}\right]^2, \tag{8}$$

$$I_{\mathrm{sig}}^{\mathrm{het}}(\tau) \propto \left[\langle \cos^2\theta \rangle_{\varphi(\tau)} - \frac{1}{3} + C\right]^2, \tag{9}$$

where θ is the angle between the molecular axis and the polarization of the field, and C represents a permanent contribution to the signal (constant) that is proportional to the electric field (110).

7.2. Single-Shot Rotational Spectroscopy

Femtosecond-duration pulses that have undergone filamentation can also be used to probe the rotational structure of the constituent gas after impulsive excitation in a single-shot configuration. In this experiment, one leverages the fact that the rotation period of a molecule (>1 ps) is typically much longer than the duration of a regeneratively amplified femtosecond laser pulse (typically of duration 35–150 fs), and the rotational motion can be excited simply using the pulse emitted by the regenerative amplifier. In fact, the criterion for impulsive excitation is that the laser pulse be of a similar order of magnitude to the pertinent motion; thus, a rotational mode can even be excited by a 1–10-ps pulse, depending on the size of the molecules of interest. The impulsive rotational response is often measured using a scanning delay line with the probe pulse interrogating a particular section of the excited medium defined by the crossing angle of the pump and probe beams and their relative positions in time. A scan typically requires several minutes to complete and provides spectral information regarding the molecules excited by the beam (110, 111). The rotational response can also be mapped onto a temporally dispersed (chirped) probe beam, for which the magnitude of the dispersion sets the temporal window accessible using a single probe pulse (112, 113). In this manner, the time delay is mapped on the spectral component that interacts with the recurring rotational response.

The spectral broadening that occurs during filamentary propagation provides an ideal source of coherent radiation spanning one or more octaves of bandwidth in the visible region using a fundamental wavelength of 800 nm. By temporally dispersing the white-light pulse generated by the filamentation process, McCole et al. (114) showed that rotational revivals excited impulsively can be probed simultaneously over a long (>65 ps) temporal window (**Figure 4**). Owing to the

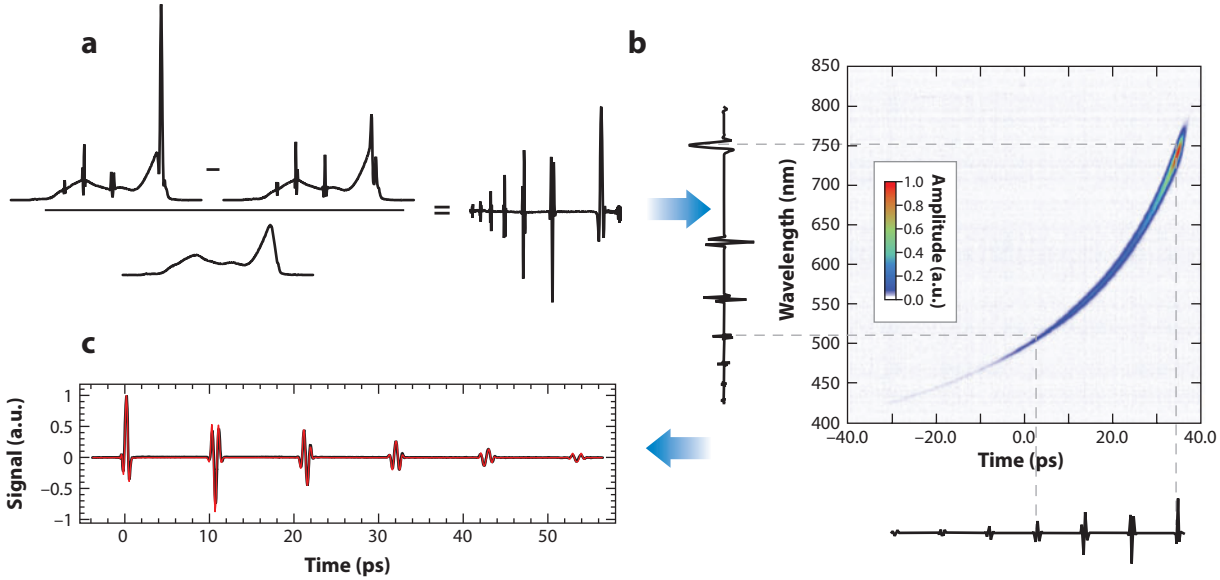

Figure 4

Principle of time-resolved rotational wave-packet spectroscopy using a chirped white-light filament as a probe. (*a*) The out-of-quadrature signal is subtracted from the in-quadrature signal and divided by the reference probe spectrum to yield the pure heterodyne signal. (*b*) The heterodyne signal is mapped via the white-light pulse group delay to yield the time-resolved signal (*c*). Figure adapted with permission from Reference 114. Copyright 2013 by the American Chemical Society.

simultaneous generation of the continuum components in the filament, the relative phases of the spectral components are well defined and depend only on the dispersion of the material encountered by the beam after the filament. In a highly dispersive glass such as SF11, a large frequency chirp can be applied to the filament pulse, enabling a significant portion of the rotational spectrum to be measured in a single laser shot. The rotational wave packets created in the molecular medium by an intense pump pulse interact with the white-light probe through cross-phase modulation-induced birefringence that is detected through a quarter-wave plate and crossed analyzer. Linear molecules, including N_2, O_2, and CO_2, were measured, as were several asymmetric tops, including ethylene and methanol.

7.3. Impulsive Stimulated Vibrational Raman Scattering

A powerful application of the natural pulse shortening that occurs during filamentation is the impulsive excitation of vibrational modes in molecular media. Such impulsive excitation occurs when the duration of the pulse becomes shorter than the characteristic vibrational period of a Raman-active mode. As detailed above, this has been used to measure the dynamics of filamentation (76), but the method can also be applied to the detection of airborne molecules. Indeed, Calegari et al. (115) first recognized the potential of time-resolved filament-assisted ISRS for molecular detection, demonstrating detection of the CO_2 Fermi doublet in an impulsive pump–impulsive probe configuration with the chirped-mirror-compressed output of a filament generated in argon. The rapid (8-fs period) vibration of H_2 was also measured in that study, facilitated by self-shortening of the pulse during propagation in the sample itself. Further investigations expanded on the method, detecting the major vibrational modes in N_2, O_2, CO_2, N_2O, CH_4, and C_2H_6, as well as the full Raman response (rotational and vibrational) of H_2 (116).

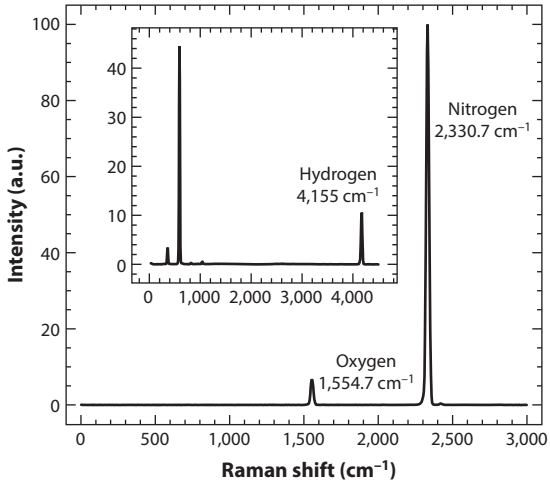

Figure 5

The vibrational spectrum of air comprising oxygen and nitrogen. (*Inset*) The rotational-vibrational Raman spectrum of hydrogen, in which all the rotational transitions ($_J|2 \leftarrow 0\rangle$, $_J|3 \leftarrow 1\rangle$, $_J|4 \leftarrow 2\rangle$, and $_J|5 \leftarrow 3\rangle$) and the fundamental vibrational transition are observed. Figure adapted with permission from Reference 139. Copyright 2011 by the American Chemical Society.

The impulsively excited Raman response can also be extracted using a frequency domain measurement, in which a picosecond-duration probe pulse interferes with the time-dependent polarizability of the medium caused by the coherent molecular motion to generate side bands via coherent anti-Stokes and Stokes Raman scattering. Odhner et al. (5) demonstrated the direct excitation of vibrations by filamentary self-shortening of a 50-fs pulse with no chirp compensation for the case of H_2 using a filament in air. In this experiment, the authors generated a narrowband probe beam using a zero-dispersion 4-*f* spectral filter composed of a grating, a cylindrical mirror, and a controllable slit in the Fourier plane of the filter. Owing to the hard edges in the spectral filter, the probe pulse exhibits a sinc^2 temporal profile, and to minimize cross-phase modulation while maximizing the probe overlap with the excited medium, the authors set the pump-probe time delay to ~750 fs (pump preceding probe), which is the first minimum in the probe temporal intensity profile. This maximizes the signal-to-noise ratio, given the relatively rapid (several picoseconds) dispersion of the vibrational wave packet for gas-phase diatomic and small polyatomic molecules. The entire spectrum is generated in a single laser pulse, and the spectrum spans the low-frequency rotational modes through the O_2 and N_2 stretch to the fastest fundamental mode of H_2 at 4,155 cm^{-1} (having an 8-fs period) (**Figure 5**). This indicates that self-shortening of the filamentary pulse has produced a temporal feature in the filament that is shorter than 8 fs. The spectrum also indicates that the method has respectable signal to noise (~10,000) in just a few milliseconds of acquisition time for the gas-phase coherent Raman process. There is no restriction on the pump or probe wavelength, or whether Stokes or anti-Stokes scattering is measured (both are observed with comparable intensity); thus, there is considerable flexibility with regard to experimental design.

Filament-driven impulsive Raman spectroscopy has also been used for time-resolved spectroscopy. In this experiment, a filament formed by focusing an ~2-mJ laser pulse through a $f =$ 2.27-m lens impulsively excited the constituent molecules in air, and the vibrational wake was then probed by a narrowband pulse at 400 nm, formed by doubling the fundamental pulse in a long β-BBO crystal. The dispersion of the rovibrational wave packet excited by the filament was fit with an analytical expression having temperature as the only variable parameter (**Figure 6**).

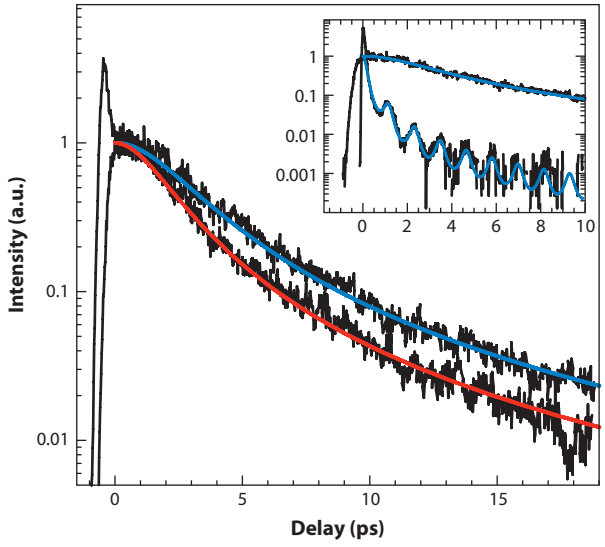

Figure 6

Time-resolved measurements of the dispersion of rovibrational wave packets excited in nitrogen (*blue fit*) and oxygen (*red fit*). The colored curves correspond to fits using Equation 10 for a temperature of 300 K. (*Inset*) Comparison of the dispersion of a wave packet in nitrogen at room temperature and at 3,000 K, corresponding to the nominal temperature of a methane flame. Figure adapted with permission Reference 5, copyright 2009 by the American Physical Society.

The time-resolved Raman signal was fit using the expression

$$I_S(t_d) \sim \frac{\left[\exp\left(\frac{2B_e}{kT}\right) + \frac{1}{2}\right]^2 - \sin^2\left(\frac{\alpha_e}{\hbar} t_d\right)}{\left[1 + \left(\frac{\alpha_e T}{B_e \hbar} t_d\right)^2\right]\left[\sinh^2\left(\frac{\hbar\omega_e}{2kT}\right) + \sin^2\left(\omega_e x_e t_d\right)\right]}, \quad (10)$$

where t_d is the pump-probe time delay, ω_e is the vibrational angular frequency, B_e is the rotational constant, α_e is the anharmonicity constant, $\omega_e x_e$ is the vibration rotation coupling constant, and k and T are the Boltzmann constant and temperature of the system, respectively. The expression is derived from a model that assumes the formation of a coherent wave packet specified by the initial distribution of rotational-vibrational states for a given molecule at a particular temperature. Thus, the temperature of the system can be probed directly by measuring the dispersion of the coherently evolving wave packet. The fit for the data for air in the filament revealed a temperature of 300 K, suggesting that no thermal energy is deposited in the vibrational degrees of freedom during filamentation on the timescale of the measurement. This is interesting given the nature of the strong field excitation. This new thermometry technique was tested using a methane-air flame produced in a Bunsen burner located below the region of pump-probe overlap (5). The excellent fit between the theoretical prediction and the Bunsen burner data shown in the inset of **Figure 6** suggests that the essential physics is captured by the derived expression for the time-dependent polarization.

Impulsive stimulated Raman vibrational spectroscopy has been performed on a series of heteronuclear polyatomic molecules in the spectral domain. **Figure 7** displays the impulsive stimulated Raman vibrational spectra for triethylamine, ammonia, nitromethane, and gasoline measured at a distance of 2.5 m from the laser system. The signal is imprinted on a picosecond-duration probe beam and is measured using a USB coupled spectrometer. The coherent nature

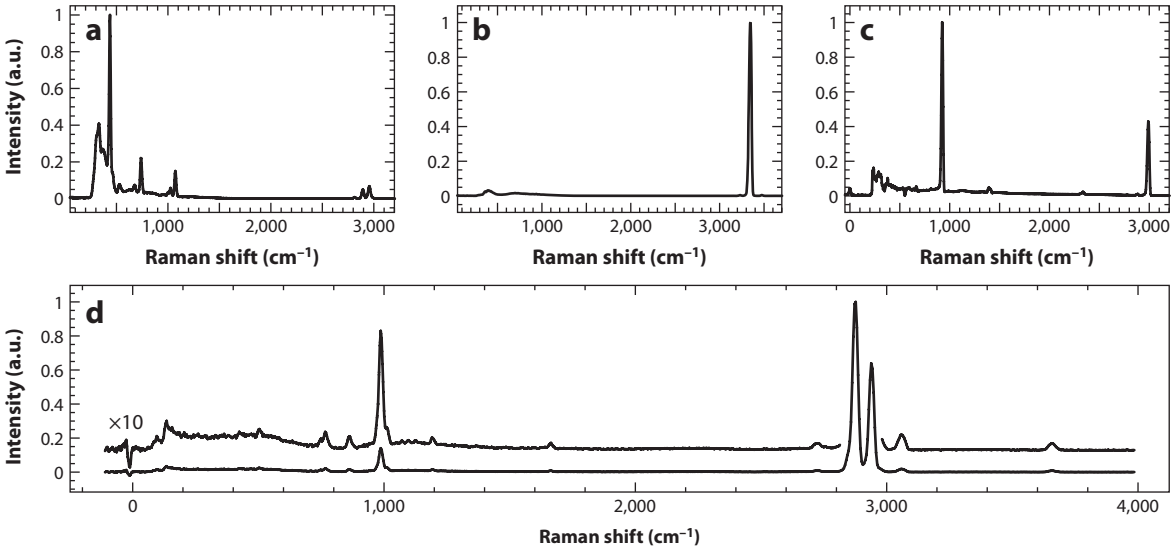

Figure 7

The Raman spectra of (*a*) triethylamine, (*b*) ammonia, (*c*) nitromethane, and (*d*) gasoline measured using gas-phase filament-driven impulsive Raman spectroscopy. Figure adapted with permission from Reference 139. Copyright 2011 by the American Chemical Society.

of the measurement can be seen in **Figure 7*d*** plotted in log space. The lineshape of the features displays a dispersive feature after the resonance. The feature results from destructive interference between the resonant and nonresonant excitation paths, which have opposite phase on the high-frequency side of the resonance.

7.4. Filament-Induced Breakdown Spectroscopy

Laser filamentation has been employed to characterize the atomic constituents in materials at standoff distances up to approximately 200 m (117). In conventional laser-induced breakdown spectroscopy, a nanosecond-duration laser with an energy of hundreds of millijoules is focused onto a solid material, causing plasma formation, ablation, and atomic emission from excited state atomic and diatomic cluster materials. Such experiments have been performed since the invention of the pulsed laser in 1962 (118). For standoff detection applications, the emission is detected using a telescope coupled to an optical spectrometer to obtain the highest sensitivity possible (119). The laser intensity at the focus must be high enough to induce plasma formation; thus for increasing standoff distances, increasingly larger lens diameters are required to obtain sufficiently small focal spot diameters. The size of the focusing lens required to induce plasma formation becomes prohibitively large for standoff distances of ~100 m. For femtosecond lasers, one can precompensate the linear chirp using a grating compressor and laser pulse shaping (120) to control the distance at which the laser will undergo filamentation and produce a high intensity. Thus, filamentation has been explored as a means to enable laser-induced breakdown spectroscopy. This approach has been termed remote filament-induced breakdown spectroscopy (121). Without filamentation, a collimated laser pulse will have insufficient energy to induce plasma formation on the material surface. However, as noted in Section 1, after Kerr lensing exceeds diffraction, intensities of the order of 10^{13} W cm^{-2} are attained, which is sufficient to induce plasma formation on the surface with concomitant ablation and plasma emission from the atomic and small molecular species.

Filament-based breakdown spectroscopy has been employed to characterize the hardness of carbon materials based on their atomic composition (10) at a standoff distance of 6 m. One important result from this investigation was the demonstration that filament-based measurements involving nonlinear processes have lower noise levels (~3 ×) in comparison with measurements that simply employ the output from the regeneratively amplified laser pulse directly. The improvement in the signal to noise was attributed to the intensity clamping that accompanies laser filamentation, providing a much more stable pulse-to-pulse intensity. Filamentation has been used to provide longer-range remote detection with the Teramobile system (117). This experiment employed a 100-mJ laser pulse to induce filamentation on solid targets at a distance of 180 m, and the detection of copper emission was easily performed. Filament-induced breakdown spectroscopy has also been used to characterize the emission from various agricultural grains at a distance of 5 m (122).

7.5. Fluorescence Emission

Investigators have used fluorescence from excited species in the filament to characterize the properties of femtosecond laser filaments and also as a remote probe of gas-phase molecules for sensing applications. The high intensity attained in the core of the filament leads to ionization and electronic excitation due to multiphoton absorption, followed by electron-ion recombination and further collisions among energetic electrons, ions, and neutral species. In a filament generated in air, such excitation leads to visible fluorescence originating mainly from the $N_2^+(B^2\Sigma_u^+ - X^2\Sigma_g^+)$ and $N_2(C^3\Pi_u - B^3\Pi_g)$ transitions (123, 124). Because of the low density of plasma generated during femtosecond laser filamentation ($n_e \approx 10^{14}$–10^{16}), bremsstrahlung emission is much weaker than that in a plasma generated by a picosecond or nanosecond pulse, which makes detecting the fluorescence emission from the filament much easier. The nitrogen fluorescence from a filament has been used to track propagation dynamics by recording the fluorescence intensity as a function of propagation distance, gas pressure, and laser intensity (18, 125).

Filament-induced fluorescence was first investigated as a means of detecting halocarbons in air. Although the fluorescence signatures of the halocarbons used in this study are typically obscured by nitrogen emission from the air, Gravel et al. (126) showed that the different emission timescales of the species can be employed to selectively detect the halocarbon emission. The N_2 fluorescence lifetime is 2 ns, so correspondingly longer gating times can be used to suppress the N_2 background. Signatures from ethanol in air up to 10 m away have also been measured using the filament-based fluorescence method, in which the high intensity of the filament was employed to dissociate ethanol into excited CH and C_2 neutral radicals that proceed to fluoresce (127). Finally, additional gas-phase hydrocarbon samples have been measured in air using filament-based fluorescence, including methane, acetylene, and clouds of smoke with a sensitivity of the order of 50 ppm in the best case (122, 128, 129). Simultaneous detection and identification of multigas pollutants have also been performed using filament-induced nonlinear spectroscopy (129–132). For a further review of filament-induced fluorescence spectroscopy, readers are referred to Reference 133.

7.6. Backward Lasing

Filamentation has been proposed as a potential means to generate coherent radiation propagating in the direction counter to that of the laser used to generate the filament. Coherent methods for generating backward propagating radiation are prohibited by momentum conservation, and thus other solutions are sought. The motivation for these investigations is that such a backward propagating beam could be used as a means to generate a measurable signal from signature molecules at considerable standoff distances (100–1,000 m). Potential detection experiments include UV-visible and vibrational absorption, stimulated Raman scattering, coherent anti-Stokes

Raman scattering, and superfluorescence (134). Backward lasing was recently demonstrated using resonance enhanced multiphoton ionization of oxygen in air with nanosecond lasers (135), in which a two-photon excitation at 226 nm dissociates O_2 and a second two-photon excitation from the $2p^3$P to the $3p^3$P state creates a population inversion with the $3s^3$S state. Amplified spontaneous emission at 845 nm from the 1-mm-long cylinder of excitation led to a coherent backward propagating pulse that in principle could be used as a seed for the detection methods listed above. However, high-intensity beams are required from geometric focusing, and thus the extension of this technique to longer distances is problematic.

Stimulated Raman scattering is under investigation as a coherent backward propagating detection technology due to the inherent phase matching and linear scaling of the signal with sample number density (136). In such an experiment, the pump and Stokes laser beams are tuned to have a frequency difference $\Omega = \omega_p - \omega_s$ equal to a characteristic vibrational level for a signature molecule. The laser beams interact with a gas-phase sample, preparing a molecular coherence that in theory interacts with the backward propagating amplified stimulated emission. In this case, the signal scales as $\mathrm{SRG} = +\mathrm{Im}(\chi^{(3)})I_pL$, where $\chi^{(3)}$ is the susceptibility of the signature molecule, I_p is the pump laser intensity from the filament, and L is the interaction length between the Stokes and the pump beams.

The primary motivation for such research is that an intensity of 10^{13} W cm^{-2} provides the opportunity to generate a population inversion in molecular species, for example, in N_2 between the C $^3\Pi_u$ and the B $^3\Pi_g$ states to produce the 337.1-nm line. If population inversion can be achieved, spontaneous emission occurring throughout the filamentation region would lead to amplification. An emission occurring at the far end of the filament (from the observer) would then undergo amplified spontaneous emission toward the observer and thus generate gain in the backward direction. In a proof-of-principle experiment, backward propagating amplified spontaneous emission was observed during filamentation in a gas-phase mixture of argon and nitrogen (24). The excited electronic states of argon created during the laser filamentation process served to transfer energy and populate the C and B states in nitrogen, forming the population inversion with the B and A states, respectively. The filament was driven by an intense, 80-fs, 3.9-μm mid-IR pulse with energies up to 8 mJ. In this experiment, the N_2 inversion was pumped by electronically excited argon atoms that were present in tenfold excess in the nitrogen gas. Lasing was detected at 337 nm and 357 nm for input energies above 7 mJ per pulse. Unfortunately, nitrogen itself will serve to quench the C state population at pressures above 1.7 bar via the N_2 (C $^2\Pi_u$) + N_2 (X $^1\Sigma_g$) → N_4 → N_2(B $^3\Pi_g$ vibrationally excited) + N_2(X$^1\Sigma_g$) relaxation pathway. Oxygen is an even more efficient quencher of excited N_2, suggesting that a free space N_2 laser in air will be challenging to create. Simulations suggest that a longer plasma channel, with a higher plasma density and larger filament diameter, contributes to enhanced lasing in the mid-IR in comparison with near-IR measurements. A previous report of backward lasing in a filament was likely attributable to fluorescence in a multifilament pump intensity at up to 170 critical powers (137).

SUMMARY POINTS

1. Laser filament is a robust nonlinear phenomenon that self-focuses and self-shortens laser pulses to durations as short as a few optical cycles and intensities exceeding 10^{13} W cm^{-2}. The phenomenon results from the interplay of Kerr lensing and plasma defocusing in femtosecond laser propagation in gas-phase media.

2. The process of laser filamentation produces a sub-10-fs coherent bandwidth at a controllable distance from the laser source.
3. Laser filamentation creates rotational revivals in air propagating at the speed of light (quantum wakes) that can serve to manipulate subsequent radiation pulses.
4. Laser filamentation induces coherent rotational and vibrational motion in molecules in air that can be detected in either the time domain (scanning pump probe) or frequency domain (single-shot frequency domain spectroscopy) that can be employed for standoff spectroscopy.
5. The propagation dynamics of laser filamentation can be measured using transient-grating, cross-polarization, frequency-resolved optical gating, and the measurements are in accord with theoretical predictions.
6. The proposed contribution of the HOKE to the propagation dynamics of laser filamentation has been shown to be negligible in both theory and experimental measurements.
7. Laser filamentation provides a potential path to backward lasing for remote sensing applications.

DISCLOSURE STATEMENT

The authors are not aware of any affiliations, memberships, funding, or financial holdings that might be perceived as affecting the objectivity of this review.

ACKNOWLEDGMENTS

We gratefully acknowledge the support of the Office of Naval Research (N00014-10-1-0293), the National Science Foundation (CHE0957694), and the Defense Threat Reduction Agency (HDTRA1-12-0014).

LITERATURE CITED

1. Couairon A, Mysyrowicz A. 2007. Femtosecond filamentation in transparent media. *Phys. Rep.* 441:47–189
2. Bergé L, Skupin S, Nuter R, Kasparian J, Wolf JP. 2008. Ultrashort filaments of light in weakly ionized, optically transparent media. *Rep. Prog. Phys.* 71:109801
3. Kasparian J, Wolf J-P. 2008. Physics and applications of atmospheric nonlinear optics and filamentation. *Opt. Express* 16:466–93
4. Varma S, Chen YH, Milchberg HM. 2008. Trapping and destruction of long-range high-intensity optical filaments by molecular quantum wakes in air. *Phys. Rev. Lett.* 101:205001
5. Odhner JH, Romanov DA, Levis RJ. 2009. Rovibrational wave-packet dispersion during femtosecond laser filamentation in air. *Phys. Rev. Lett.* 103:075005
6. Nibbering ETJ, Grillon G, Franco MA, Prade BS, Mysyrowicz A. 1997. Determination of the inertial contribution to the nonlinear refractive index of air, N_2, and O_2 by use of unfocused high-intensity femtosecond laser pulses. *J. Opt. Soc. Am. B* 14:650–60
7. Zheltikov AM. 2007. Raman response function of atmospheric air. *Opt. Lett.* 32:2052–54
8. Wahlstrand JK, Cheng YH, Milchberg HM. 2012. Absolute measurement of the transient optical nonlinearity in N_2, O_2, N_2O, and Ar. *Phys. Rev. A* 85:043820

9. Rodriguez M, Sauerbrey R, Wille H, Wöste L, Fujii T, et al. 2002. Triggering and guiding megavolt discharges by use of laser-induced ionized filaments. *Opt. Lett.* 27:772–74
10. Judge EJ, Heck G, Cerkez EB, Levis RJ. 2009. Discrimination of composite graphite samples using remote filament-induced breakdown spectroscopy. *Anal. Chem.* 81:2658–63
11. Brady JJ, Judge EJ, Levis RJ. 2009. Mass spectrometry of intact neutral macromolecules using intense non-resonant femtosecond laser vaporization with electrospray post-ionization. *Rapid Commun. Mass Spectrom.* 23:3151–57
12. Brady JJ, Judge EJ, Levis RJ. 2011. Nonresonant femtosecond laser vaporization of aqueous protein preserves folded structure. *Proc. Natl. Acad. Sci. USA* 108:12217–22
13. Perez JJ, Flanigan PM, Brady JJ, Levis RJ. 2013. Classification of smokeless powders using laser electrospray mass spectrometry and offline multivariate statistical analysis. *Anal. Chem.* 85:296–302
14. Braun A, Korn G, Liu X, Du D, Squier J, Mourou G. 1995. Self-channeling of high-peak-power femtosecond laser pulses in air. *Opt. Lett.* 20:73–75
15. Marburger J. 1975. Self-focusing: theory. *Prog. Quantum Electron.* 4:35–110
16. Hauri CP, Kornelis W, Helbing FW, Heinrich A, Couairon A, et al. 2004. Generation of intense, carrier-envelope phase-locked few-cycle laser pulses through filamentation. *Appl. Phys. B* 79:673–77
17. Stibenz G, Zhavoronkov N, Steinmeyer G. 2006. Self-compression of millijoule pulses to 7.8 fs duration in a white-light filament. *Opt. Lett.* 31:274–76
18. Becker A, Aközbek N, Vijayalakshmi K, Oral E, Bowden CM, Chin SL. 2001. Intensity clamping and re-focusing of intense femtosecond laser pulses in nitrogen molecular gas. *Appl. Phys. B* 73:287–90
19. Schwarz J, Rambo P, Diels JC, Kolesik M, Wright EM, Moloney JV. 2000. Ultraviolet filamentation in air. *Opt. Commun.* 180:383–90
20. Tzortzakis S, Lamouroux B, Chiron A, Franco M, Prade B, et al. 2000. Nonlinear propagation of subpicosecond ultraviolet laser pulses in air. *Opt. Lett.* 25:1270–72
21. Hauri CP, Lopez-Martens RB, Blaga CI, Schultz KD, Cryan J, et al. 2007. Intense self-compressed, self-phase-stabilized few-cycle pulses at 2 μm from an optical filament. *Opt. Lett.* 32:868–70
22. Muecke OD, Ališauskas S, Verhoef AJ, Pugžlys A, Baltuska A, et al. 2009. Self-compression of millijoule 1.5 μm pulses. *Opt. Lett.* 34:2498–500
23. Kartashov D, Ališauskas S, Pugžlys A, Voronin A, Zheltikov A, et al. 2013. Mid-infrared laser filamentation in molecular gases. *Opt. Lett.* 38:3194–97
24. Kartashov D, Ališauskas S, Andriukaitis G, Pugžlys A, Shneider M, et al. 2012. Free-space nitrogen gas laser driven by a femtosecond filament. *Phys. Rev. A* 86:033831
25. Askaryan G. 1962. Effect of the gradient of a strong electromagnetic ray on electrons and atoms. *Zh. Eksp. Teor. Fiz.* 42:1567–70
26. Hercher M. 1964. Laser-induced damage in transparent media. *J. Opt. Soc. Am.* 54:563
27. Chiao RY, Garmire E, Townes CH. 1964. Self-trapping of optical beams. *Phys. Rev. Lett.* 13:479–82
28. Dyshko AL, Lugovoi VN, Prokhorov AM. 1967. Self-focusing of intense light beams. *JETP Lett.* 6:146–48
29. Shen Y-R, Marburger J. 1975. *Self-Focusing: Experimental*. New York: Pergamon
30. Alfano RR, Shapiro SL. 1970. Emission in region 4000 to 7000 Å via four-photon coupling in glass. *Phys. Rev. Lett.* 24:584–87
31. Alfano RR, Shapiro SL. 1970. Observation of self-phase modulation and small-scale filaments in crystals and glasses. *Phys. Rev. Lett.* 24:592–94
32. Alfano RR, Shapiro SL. 1970. Direct distortion of electronic clouds of rare-gas atoms in intense electric fields. *Phys. Rev. Lett.* 24:1217–20
33. Gustafson TK, Taran JP, Haus HA, Lifsitz JR, Kelley PL. 1969. Self-modulation self-steepening and spectral development of light in small-scale trapped filaments. *Phys. Rev.* 177:306–13
34. Bloembergen N. 1973. The influence of electron plasma formation on superbroadening in light filaments. *Opt. Commun.* 8:285–88
35. Alfano RR, Shapiro SL. 1971. Picosecond spectroscopy using the inverse Raman effect. *Chem. Phys. Lett.* 8:631–33
36. Fork RL, Shank CV, Hirlimann C, Yen R, Tomlinson WJ. 1983. Femtosecond white-light continuum pulses. *Opt. Lett.* 8:1–3

37. Miller RI, Roberts TG. 1987. Laser self-focusing in the atmosphere. *Appl. Opt.* 26:4570–75
38. Kühlke D, Herpers U, von der Linde D. 1987. Spectral broadening of intense femtosecond pulses in atmospheric air. *Opt. Commun.* 63:275–77
39. Strickland D, Mourou G. 1985. Compression of amplified chirped optical pulses. *Opt. Commun.* 55:447–49
40. Squier J, Salin F, Mourou G, Harter D. 1991. 100-fs pulse generation and amplification in Ti-Al_2O_3. *Opt. Lett.* 16:324–26
41. Kmetec JD, Macklin JJ, Young JF. 1991. 0.5-TW, 125-fs Ti-sapphire laser. *Opt. Lett.* 16:1001–3
42. Sullivan A, Hamster H, Kapteyn HC, Gordon S, White W, et al. 1991. Multiterawatt, 100-fs laser. *Opt. Lett.* 16:1406–8
43. Umstader D, Liu X. 1992. Self-guiding of high-intensity laser pulses for laser wake field acceleration. *AIP Conf. Proc.* 279:450–60
44. Zhao XM, Diels JC, Wang CY, Elizondo JM. 1995. Femtosecond ultraviolet-laser pulse induced lightning discharges in gases. *IEEE J. Quantum Electron.* 31:599–612
45. Zhao XM, Rambo P, Diels JC. 1995. Quantum electronics and lasers. *Proc. 1995 OSA Tech. Dig. Ser.*, pp. 178–79. Washington, DC: Opt. Soc. Am.
46. Nibbering ETJ, Curley PF, Grillon G, Prade BS, Franco MA, et al. 1996. Conical emission from self-guided femtosecond pulses in air. *Opt. Lett.* 21:62–64
47. Brodeur A, Chien CY, Ilkov FA, Chin SL, Kosareva OG, Kandidov VP. 1997. Moving focus in the propagation of ultrashort laser pulses in air. *Opt. Lett.* 22:304–6
48. Couairon A, Biegert J, Hauri CP, Kornelis W, Helbing FW, et al. 2006. Self-compression of ultra-short laser pulses down to one optical cycle by filamentation. *J. Mod. Optics* 53:75–85
49. Prade B, Franco M, Mysyrowicz A, Couairon A, Buersing H, et al. 2006. Spatial mode cleaning by femtosecond filamentation in air. *Opt. Lett.* 31:2601–3
50. Lange HR, Grillon G, Ripoche JF, Franco MA, Lamouroux B, et al. 1998. Anomalous long-range propagation of femtosecond laser pulses through air: moving focus or pulse self-guiding? *Opt. Lett.* 23:120–22
51. Mlejnek M, Wright EM, Moloney JV. 1999. Moving-focus versus self-waveguiding model for long-distance propagation of femtosecond pulses in air. *IEEE J. Quantum Electron.* 35:1771–76
52. Mlejnek M, Wright EM, Moloney JV. 1998. Dynamic spatial replenishment of femtosecond pulses propagating in air. *Opt. Lett.* 23:382–84
53. Mlejnek M, Kolesik M, Moloney JV, Wright EM. 1999. Optically turbulent femtosecond light guide in air. *Phys. Rev. Lett.* 83:2938–41
54. Mlejnek M, Wright EM, Moloney JV. 1999. Power dependence of dynamic spatial replenishment of femtosecond pulses propagating in air. *Opt. Express* 4:223–28
55. Brabec T, Krausz F. 1997. Nonlinear optical pulse propagation in the single-cycle regime. *Phys. Rev. Lett.* 78:3282–85
56. Bergé L, Skupin S, Nuter R, Kasparian J, Wolf JP. 2007. Ultrashort filaments of light in weakly ionized, optically transparent media. *Rep. Prog. Phys.* 70:1633–713
57. Couairon A, Brambilla E, Corti T, Majus D, de J. Ramírez-Góngora O, Kolesik M. 2011. Practitioner's guide to laser pulse propagation models and simulation. *Eur. Phys. J. Spec. Top.* 199:5–76
58. Sprangle P, Peñano JR, Hafizi B. 2002. Propagation of intense short laser pulses in the atmosphere. *Phys. Rev. E* 66:046418
59. Ripoche JF, Grillon G, Prade B, Franco M, Nibbering E, et al. 1997. Determination of the time dependence of N_2 in air. *Opt. Commun.* 135:310–14
60. Zheltikov AM. 2008. An analytical model of the rotational Raman response function of molecular gases. *J. Raman Spectrosc.* 39:756–65
61. Palastro JP, Antonsen TM Jr, Milchberg HM. 2012. Compression, spectral broadening, and collimation in multiple, femtosecond pulse filamentation in atmosphere. *Phys. Rev. A* 86:033834
62. Nurhuda M, Suda A, Midorikawa K. 2008. Generalization of the Kerr effect for high intensity, ultrashort laser pulses. *New J. Phys.* 10:053006
63. Béjot P, Kasparian J, Henin S, Loriot V, Vieillard T, et al. 2010. Higher-order Kerr terms allow ionization-free filamentation in gases. *Phys. Rev. Lett.* 104:103903

64. Kasparian J, Béjot P, Wolf J-P. 2010. Arbitrary-order nonlinear contribution to self-steepening. *Opt. Lett.* 35:2795–97
65. Wang Z, Zhang C, Liu J, Li R, Xu Z. 2011. Femtosecond filamentation in argon and higher-order nonlinearities. *Opt. Lett.* 36:2336–38
66. Béjot P, Kasparian J. 2011. Conical emission from laser filaments and higher-order Kerr effect in air. *Opt. Lett.* 36:4812–14
67. Petrarca M, Petit Y, Henin S, Delagrange R, Béjot P, Kasparian J. 2012. Higher-order Kerr improve quantitative modeling of laser filamentation. *Opt. Lett.* 37:4347–49
68. Wang H, Fan C, Zhang P, Qiao C, Zhang J, Ma H. 2011. Dynamics of femtosecond filamentation with higher-order Kerr response. *J. Opt. Soc. Am. B* 28:2081–86
69. Brée C, Demircan A, Skupin S, Bergé L, Steinmeyer G. 2009. Self-pinching of pulsed laser beams during filamentary propagation. *Opt. Express* 17:16429–35
70. Brée C, Demircan A, Skupin S, Bergé L, Steinmeyer G. 2010. Plasma induced pulse breaking in filamentary self-compression. *Laser Phys.* 20:1107–13
71. Loriot V, Hertz E, Faucher O, Lavorel B. 2009. Measurement of high order Kerr refractive index of major air components. *Opt. Express* 17:13429–34
72. Wahlstrand JK, Milchberg HM. 2011. Effect of a plasma grating on pump-probe experiments near the ionization threshold in gases. *Opt. Lett.* 36:3822–24
73. Odhner JH, Romanov DA, McCole ET, Wahlstrand JK, Milchberg HM, Levis RJ. 2012. Ionization-grating-induced nonlinear phase accumulation in spectrally resolved transient birefringence measurements at 400 nm. *Phys. Rev. Lett.* 109:065003
74. Wahlstrand JK, Odhner JH, McCole ET, Cheng YH, Palastro JP, et al. 2013. Effect of two-beam coupling in strong-field optical pump-probe experiments. *Phys. Rev. A* 87:053801
75. Köhler C, Guichard R, Lorin E, Chelkowski S, Bandrauk AD, et al. 2013. Saturation of the nonlinear refractive index in atomic gases. *Phys. Rev. A* 87:043811
76. Odhner JH, Romanov DA, Levis RJ. 2010. Self-shortening dynamics measured along a femtosecond laser filament in air. *Phys. Rev. Lett.* 105:125001
77. Yan YX, Gamble EB, Nelson KA. 1985. Impulsive stimulated scattering: general importance in femtosecond laser-pulse interactions with matter, and spectroscopic applications. *J. Chem. Phys.* 83:5391–99
78. Bernstein AC, Diels JC, Luk TS, Nelson TR, McPherson A, Cameron SM. 2003. Time-resolved measurements of self-focusing pulses in air. *Opt. Lett.* 28:2354–56
79. Adams DE, Planchon TA, Squier JA, Durfee CG. 2010. Spatiotemporal dynamics of ionizing filaments in air. In *Lasers and Electro-Opt. Quantum Electron. Laser Sci. Conf.*, JThE119. Washington, DC: Opt. Soc. Am.
80. Liu W CS. 2005. Direct measurement of the critical power of femtosecond Ti:sapphire laser pulse in air. *Opt. Lett.* 13:5750–55
81. Brée C, Bethge J, Skupin S, Bergé L, Demircan A, Steinmeyer G. 2010. Cascaded self-compression of femtosecond pulses in filaments. *New J. Phys.* 12:093046
82. Kasparian J, Sauerbrey R, Chin SL. 2000. The critical laser intensity of self-guided light filaments in air. *Appl. Phys. B* 71:877–79
83. Talebpour A, Petit S, Chin SL. 1999. Re-focusing during the propagation of a focused femtosecond Ti:sapphire laser pulse in air. *Opt. Commun.* 171:285–90
84. Hauri CP, Guandalini A, Eckle P, Kornelis W, Biegert J, Keller U. 2005. Generation of intense few-cycle laser pulses through filamentation: parameter dependence. *Opt. Express* 13:7541–47
85. Théberge F, Aközbek N, Liu WW, Becker A, Chin SL. 2006. Tunable ultrashort laser pulses generated through filamentation in gases. *Phys. Rev. Lett.* 97:023904
86. Chin SL, Théberge F, Liu W. 2007. Filamentation nonlinear optics. *Appl. Phys. B* 86:477–83
87. Dharmadhikari AK, Dharmadhikari JA, Rajgara FA, Mathur D. 2008. Polarization and energy stability of filamentation-generated few-cycle pulses. *Opt. Express* 16:7083–90
88. Xu S, Zhang Y, Liu W, Chin SL. 2009. Experimental confirmation of high-stability of fluorescence in a femtosecond laser filament in air. *Opt. Commun.* 282:4800–4
89. Bernhardt J, Liu W, Chin SL, Sauerbrey R. 2008. Pressure independence of intensity clamping during filamentation: theory and experiment. *Appl. Phys. B* 91:45–48

90. Kosareva OG, Liu W, Panov NA, Bernhardt J, Ji Z, et al. 2009. Can we reach very high intensity in air with femtosecond PW laser pulses? *Laser Phys.* 19:1776–92
91. Xu S, Bernhardt J, Sharifi M, Liu W, Chin SL. 2012. Intensity clamping during laser filamentation by TW level femtosecond laser in air and argon. *Laser Phys.* 22:195–202
92. Walter D, Eyring S, Lohbreier J, Spitzenpfeil R, Spielmann C. 2007. Spatial optimization of filaments. *Appl. Phys. B* 88:175–78
93. Nishioka H, Odajima W, Ueda K, Takuma H. 1995. Ultrabroadband flat continuum generation in multichannel propagation of terrawatt Ti:sapphire laser pulses. *Opt. Lett.* 20:2505–7
94. Aközbek N, Trushin SA, Baltuska A, Fuß W, Goulielmakis E, et al. 2006. Extending the supercontinuum spectrum down to 200 nm with few-cycle pulses. *New J. Phys.* 8:177
95. Fuji T, Horio T, Suzuki T. 2007. Generation of 12 fs deep-ultraviolet pulses by four-wave mixing through filamentation in neon gas. *Opt. Lett.* 32:2481–83
96. Kosma K, Trushin SA, Schmid WE, Fuß W. 2008. Vacuum ultraviolet pulses of 11 fs from fifth-harmonic generation of a Ti:sapphire laser. *Opt. Lett.* 33:723–25
97. Kasparian J, Sauerbrey R, Mondelain D, Niedermeier S, Yu J, et al. 2000. Infrared extension of the supercontinuum generated by femtosecond terawatt laser pulses propagating in the atmosphere. *Opt. Lett.* 25:1397–99
98. Tzortzakis S, Mechain G, Patalano G, Andre YB, Prade B, et al. 2002. Coherent subterahertz radiation from femtosecond infrared filaments in air. *Opt. Lett.* 27:1944–46
99. Fuji T, Suzuki T. 2007. Generation of sub-two-cycle mid-infrared pulses by four-wave mixing through filamentation in air. *Opt. Lett.* 32:3330–32
100. Théberge F, Châteauneuf M, Ross V, Mathieu P, Dubois J. 2008. Ultrabroadband conical emission generated from the ultraviolet up to the far-infrared during the optical filamentation in air. *Opt. Lett.* 33:2515–17
101. Théberge F, Châteauneuf M, Roy G, Mathieu P, Dubois J. 2010. Generation of tunable and broadband far-infrared laser pulses during two-color filamentation. *Phys. Rev. A* 81:033821
102. Fuji T, Nomura Y. 2013. Generation of phase-stable sub-cycle mid-infrared pulses from filamentation in nitrogen. *Appl. Sci.* 3:122–38
103. Stapelfeldt H, Seideman T. 2003. Colloquium: aligning molecules with strong laser pulses. *Rev. Mod. Phys.* 75:543–57
104. Calegari F, Vozzi C, Gasilov S, Benedetti E, Sansone G, et al. 2008. Rotational Raman effects in the wake of optical filamentation. *Phys. Rev. Lett.* 100:123006
105. Calegari F, Vozzi C, Stagira S. 2009. Optical propagation in molecular gases undergoing filamentation-assisted field-free alignment. *Phys. Rev. A* 79:023827
106. Varma S, Chen YH, Milchberg HM. 2009. Quantum molecular lensing of femtosecond laser optical/plasma filaments. *Phys. Plasmas* 16:056702
107. Béjot P, Petit Y, Bonacina L, Kasparian J, Moret M, Wolf JP. 2008. Ultrafast gaseous "half-wave plate." *Opt. Express* 16:7564–70
108. Chen Y, Marceau C, Théberge F, Châteauneuf M, Dubois J, Chin SL. 2008. Polarization separator created by a filament in air. *Opt. Lett.* 33:2731–33
109. Marceau C, Chen Y, Théberge F, Châteauneuf M, Dubois J, Chin SL. 2009. Ultrafast birefringence induced by a femtosecond laser filament in gases. *Opt. Lett.* 34:1417–19
110. Renard V, Renard M, Guérin S, Pashayan YT, Lavorel B, et al. 2003. Postpulse molecular alignment measured by a weak field polarization technique. *Phys. Rev. Lett.* 90:153601
111. Rosca-Pruna F, Vrakking MJJ. 2001. Experimental observation of revival structures in picosecond laser-induced alignment of I_2. *Phys. Rev. Lett.* 87:153902
112. Zamith S, Ansari Z, Lepine F, Vrakking MJJ. 2005. Single-shot measurement of revival structures in femtosecond laser-induced alignment of molecules. *Opt. Lett.* 30:2326–28
113. Chen YH, Varma S, York A, Milchberg HM. 2007. Single-shot, space- and time-resolved measurement of rotational wavepacket revivals in H_2, D_2, N_2, O_2, and N_2O. *Opt. Express* 15:11341–57
114. McCole ET, Odhner JH, Romanov DA, Levis RJ. 2013. Spectral-to-temporal amplitude mapping polarization spectroscopy of rotational transients. *J. Phys. Chem. A* 117:6354–61

115. Calegari F, Vozzi C, De Silvestri S, Stagira S. 2008. Molecular rotovibrational dynamics excited in optical filamentation. *Opt. Lett.* 33:2922–24
116. Calegari F, Vozzi C, Negro M, De Silvestri S, Stagira S. 2010. Filamentation-assisted time-resolved Raman spectroscopy in molecular gases. *J. Mod. Opt.* 57:967–76
117. Rohwetter P, Stelmaszczyk K, Wöste L, Ackermann R, Mejean G, et al. 2005. Filament-induced remote surface ablation for long range laser-induced breakdown spectroscopy operation. *Spectrochim. Acta B* 60:1025–33
118. Brech F, Cross L. 1962. Optical microemission stimulated by a ruby maser. *Appl. Spectrosc.* 16:59–64
119. Miziolek AW, Palleschi V, Schechter I, eds. 2006. *Laser-Induced Breakdown Spectroscopy*. Cambridge, UK: Cambridge Univ. Press
120. Heck G, Sloss J, Levis RJ. 2006. Adaptive control of the spatial position of white light filaments in an aqueous solution. *Opt. Commun.* 259:216–22
121. Stelmaszczyk K, Rohwetter P, Mejean G, Yu J, Salmon E, et al. 2004. Long-distance remote laser-induced breakdown spectroscopy using filamentation in air. *Appl. Phys. Lett.* 85:3977–79
122. Xu HL, Mejean G, Liu W, Kamali Y, Daigle JF, et al. 2007. Remote detection of similar biological materials using femtosecond filament-induced breakdown spectroscopy. *Appl. Phys. B* 87:151–56
123. Becker A, Bandrauk AD, Chin SL. 2001. S-matrix analysis of non-resonant multiphoton ionisation of inner-valence electrons of the nitrogen molecule. *Chem. Phys. Lett.* 343:345–50
124. Xu HL, Azarm A, Bernhardt J, Kamali Y, Chin SL. 2009. The mechanism of nitrogen fluorescence inside a femtosecond laser filament in air. *Chem. Phys.* 360:171–75
125. Bernhardt J, Liu W, Théberge F, Xu HL, Daigle JF, et al. 2008. Spectroscopic analysis of femtosecond laser plasma filament in air. *Opt. Commun.* 281:1268–74
126. Gravel JF, Luo Q, Boudreau D, Tang XP, Chin SL. 2004. Sensing of halocarbons using femtosecond laser-induced fluorescence. *Anal. Chem.* 76:4799–805
127. Luo Q, Xu HL, Hosseini SA, Daigle JF, Théberge F, et al. 2006. Remote sensing of pollutants using femtosecond laser pulse fluorescence spectroscopy. *Appl. Phys. B* 82:105–9
128. Xu HL, Daigle JF, Luo Q, Chin SL. 2006. Femtosecond laser-induced nonlinear spectroscopy for remote sensing of methane. *Appl. Phys. B* 82:655–58
129. Daigle JF, Kamali Y, Roy G, Chin SL. 2008. Remote filament-induced fluorescence spectroscopy from thin clouds of smoke. *Appl. Phys. B* 93:759–62
130. Xu HL, Kamali Y, Marceau C, Simard PT, Liu W, et al. 2007. Simultaneous detection and identification of multigas pollutants using filament-induced nonlinear spectroscopy. *Appl. Phys. Lett.* 90:101106
131. Kamali Y, Daigle JF, Théberge F, Châteauneuf M, Azarm A, et al. 2009. Remote sensing of trace methane using mobile femtosecond laser system of T&T Lab. *Opt. Commun.* 282:2062–65
132. Daigle JF, Kamali Y, Châteauneuf M, Tremblay G, Théberge F, et al. 2009. Remote sensing with intense filaments enhanced by adaptive optics. *Appl. Phys. B* 97:701–13
133. Chin SL, Xu HL, Luo Q, Théberge F, Liu W, et al. 2009. Filamentation "remote" sensing of chemical and biological agents/pollutants using only one femtosecond laser source. *Appl. Phys. B* 95:1–12
134. Kocharovsky V, Cameron S, Lehmann K, Lucht R, Miles R, et al. 2005. Gain-swept superradiance applied to the stand-off detection of trace impurities in the atmosphere. *Proc. Natl. Acad. Sci. USA* 102:7806–11
135. Dogariu A, Michael JB, Scully MO, Miles RB. 2011. High-gain backward lasing in air. *Science* 331:442–45
136. Malevich PN, Kartashov D, Pu Z, Ališauskas S, Pugžlys A, et al. 2012. Ultrafast-laser-induced backward stimulated Raman scattering for tracing atmospheric gases. *Opt. Express* 20:18784–94
137. Luo Q, Liu W, Chin SL. 2003. Lasing action in air induced by ultra-fast laser filamentation. *Appl. Phys. B* 76:337–40
138. Odhner J, Levis RJ. 2012. Direct phase and amplitude characterization of femtosecond laser pulses undergoing filamentation in air. *Opt. Lett.* 37:1775–77
139. Odhner JH, McCole ET, Levis RJ. 2011. Filament-driven impulsive Raman spectroscopy. *J. Phys. Chem. A* 115:13407–12